Appl. Phys. B 78, 673–676 (2004)
DOI: 10.1007/s00340-004-1519-1

Applied Physics B
Lasers and Optics

A.A. KOSTEREV[1,✉]
Y.A. BAKHIRKIN[1]
F.K. TITTEL[1]
S. BLASER[2]
Y. BONETTI[2]
L. HVOZDARA[2]

Photoacoustic phase shift as a chemically selective spectroscopic parameter

[1] Rice Quantum Institute, Rice University, Houston, TX 77251-1892, USA
[2] Alpes Lasers, 2001 Neuchatel, Switzerland

Received: 11 March 2004
Published online: 8 April 2004 •

ABSTRACT The phase information obtained in photoacoustic experiments can be used to separate the signals originating from chemical species with overlapping absorption spectra. This approach was applied to quantify parts per million CO levels in propylene using quartz-enhanced photoacoustic spectroscopy and a quantum cascade laser as an excitation source. The experimental data were used to evaluate V–T relaxation rates of CO and N_2O in propylene.

PACS 42.62.Fi; 43.35.Sx

Ultrasensitive chemical analysis of compounds in the gas phase based on molecular absorption in the mid-IR region is a well-established approach. A number of techniques have been developed to measure absorption coefficients as low as $\alpha = 10^{-9}$ cm^{-1} or less, allowing in some cases quantification of chemical species at pptv concentration levels. However, absorption-based spectroscopic methods have certain limitations. The availability of isolated absorption lines without significant background is an essential condition for high chemical selectivity and sensitivity of absorption spectroscopy. This requirement can usually be satisfied for simple molecules ($\leqslant$ 5 atoms) but not for more complex organic compounds where a high density of vibrational states and line broadening often result in structured continuum absorption over a wide spectral region. In such cases, the detection of impurities for which the absorption lines are imbedded in the continuum of the major constituent is problematical. Then the knowledge of optical absorption is not sufficient, and additional parameters are necessary to ensure chemically selective concentration measurements.

A similar problem occurs in microscopy of biological objects, where optical density alone can not reveal details of chemical composition. One of the techniques used to obtain more informative images is fluorescence lifetime imaging microscopy (FLIM) [1]. The fluorescence lifetime can be derived either from the decay curve following the excitation pulse, or from the fluorescence intensity phase shift with respect to harmonically modulated excitation. In a conceptually similar manner, the relaxation rate of optically excited molecular vibrations can be used to enhance chemical selectivity of IR measurements. As was first pointed out by G. Gorelik in 1946 [2], the phase shift of the photoacoustic response (usually called "optoacoustic", or "optic acoustic" in earlier publications) to the modulated excitation can be used as a means to measure the V–T relaxation rate. In the case of a two-level molecular system the photoacoustic phase lag θ is determined by:

$$\tan\theta = \omega\tau\,(C_{\mathrm{tr}}/C_0) \qquad (1)$$

where ω is the modulation frequency of the vibrational energy input, τ is the V–T relaxation time, C_{tr} is the translational-rotational heat capacity at constant volume, and C_0 is the total heat capacity at constant volume [3]. This was first experimentally confirmed in [4] and generalized to energy transfer processes in multilevel and multispecies systems in several subsequent studies, such as [5–7]. However, to the best of our knowledge photoacoustic phase information has not been used previously to distinguish between different gaseous components in a multi-component mixture. In most previous works when photoacoustic spectroscopy (PAS) was applied to gas sensing, the modulation frequency of the applied optical excitation was chosen so that $\omega \ll 1/\tau$ in order to obtain the highest sensitivity and the relaxation rate information was lost.

The principle of photoacoustic phase-selective detection (PPSD) is illustrated in Fig. 1. Photoacoustic signals of the two species are represented by their complex amplitudes $R_k \exp(i\varphi_k)$, $k = 1, 2$. Projections of these vectors to the axes X and Y are the experimentally observed quadrature components when the lock-in amplifier phase is referenced to the laser driver modulation input. The phase angles φ_k depend on the relaxation phase lags θ_k as determined by (1) and on the instrument lag ψ resulting from phase shifts in the electronics, the optical source and the acoustic transducer. All the delays result in clockwise rotation of the vectors (negative angles), but in Fig. 1 $\psi > \pi$ resulting in seemingly positive φ_k. This corresponds to our actual experimental conditions. If the reference frame XY is rotated so that the new X' axis is orthogonal to vector $\boldsymbol{R}_1$, then the corresponding quadrature component will contain only the $\boldsymbol{R}_2$ pro-

✉ Fax: +1-713/348-5686, E-mail: akoster@rice.edu

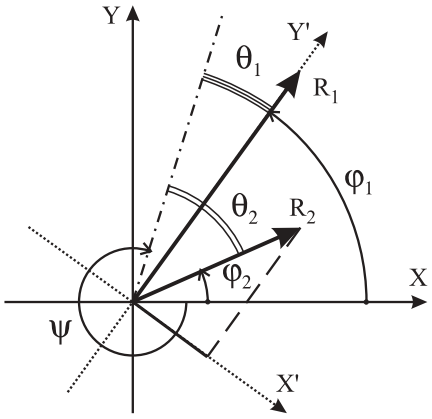

FIGURE 1 Photoacoustic signals $R_k \exp(i\varphi_k)$, shown in the complex plane. $k = 1, 2$ represents the numbering of the chemical species. The *chain line* shows the phase of photoacoustic signal which would be observed if the V–T relaxation is instantaneous

jection, allowing interference-free detection of species 2.

In this work the concept of chemical selectivity based on the difference in V–T relaxation rate was applied to detection of CO in propylene (also called propene, C_3H_6). Propylene is the monomer used in the production of polypropylene and CO impurity in the monomer feed poisons the catalyst. The high density of rovibrational states of C_3H_6 give rise to broadband structured absorption over the portion of the mid-IR region in which the CO fundamental band lies hampering the detection of CO by means of absorption spectroscopy. Figure 2 shows a portion of the IR propylene absorption spectrum available from the NIST Chemistry Webbook [8], with a 4 cm^{-1} resolution at an unspecified pressure. The shaded area indicates the CO absorption band. Our high-resolution measurements confirm that the C_3H_6 absorption interferes strongly with the detection of CO in a multipass optical cell. C_3H_6 absorption ranges from 70% to 80% in the 2173–2180 cm^{-1} spectral region at 20 Torr pressure and 100 m optical pathlength. Hence, an additional discriminating parameter is required for reliable CO quantification in a C_3H_6 host gas.

The recently introduced quartz enhanced PAS (QEPAS) [9] was used in our experiments. QEPAS is better suited for PPSD than traditional PAS [10] for two reasons. First, its operating frequency of $\sim 32\,760$ Hz is much higher than the ~ 1000 Hz characteristic frequency for traditional PAS. Second, the highest QEPAS sensitivity for absorption is achieved at a reduced pressures $P < 100$ Torr. The relaxation time is longer at reduced pressure than at atmospheric pressure because $\tau \sim 1/P$. These two features make the condition $\omega \geqslant 1/\tau$ satisfied for a wider range of molecular systems, resulting in an observable θ.

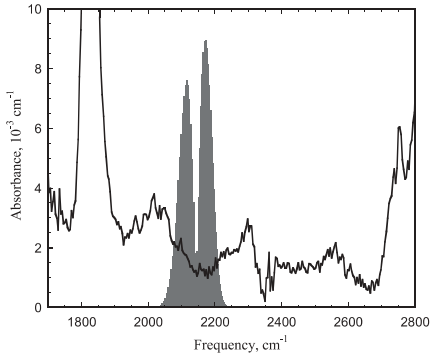

FIGURE 2 Absorption of propylene (*solid line*) and CO (*shaded area*). The *vertical axis* and *scale* refers to propylene only

The QEPAS sensor was described elsewhere in detail in Refernces [9, 11]. Briefly, a quartz tuning fork (TF) with a resonance frequency $f_0 \sim 32\,760$ Hz is used as an acoustic transducer (i.e. a microphone). In order to enhance the photoacoustic pressure, an acoustic microresonator is added. The microresonator consists of two glass tubes, each 2.45 mm long with a 0.32 mm inner diameter, aligned with the laser beam perpendicular to the TF plane. The laser wavelength is modulated at $f_0/2$ frequency with an amplitude sufficient to cover the CO absorption line. The piezoelectric current generated by the TF is converted to voltage by means of a transimpedance preamplifier and subsequently rectified at f_0 frequency in a lock-in amplifier.

A liquid-nitrogen cooled cw quantum cascade distributed feedback laser (QC-DFB) was used as an excitation source. This single-frequency laser was current-tunable in the 2195.5–2198.2 cm^{-1} range and emitted ~ 10 mW at 2196.664 cm^{-1}, which corresponds to the frequency of the R(14) CO fundamental transition [12]. Wavelength modulation was achieved by adding a harmonic dither to the QC laser current. The laser power delivered to the TF was ~ 6.5 mW.

A sample of propylene with 4.99 parts per 10^6 by volume (ppmv) of CO as specified by the supplier (Scott Specialty Gases, Inc.) was used in these studies. The QEPAS spectrum of the sample acquired at $P = 50$ Torr, 65 sccm flow and $\tau = 1$ s lock-in amplifier time constant is shown in Fig. 3a. The signal is represented by two quadrature components X and Y. The presence of an isolated CO absorption line is not evident on the C_3H_6 background. However, a rotation of the reference frame to the angle $\alpha = 22.3°$ resulted in the data representation as shown in Fig. 3b, where the X' component is free from the C_3H_6 input. The R(14) absorption line of CO is now clearly distinct with the estimated SNR = 50 (1σ). Since $\alpha = \varphi_1 - 90°$ (indices 1 and 2 will refer to C_3H_6 and CO, respectively), $\varphi_1 = 112.3°$. Similar measurements and data processing were carried out at different pressures in the 30 Torr to 150 Torr range, and it was found that a pressure of 50 Torr results in the highest CO signal component orthogonal to C_3H_6.

The rotation angle was manually adjusted in this study. However, it is possible to incorporate this procedure into

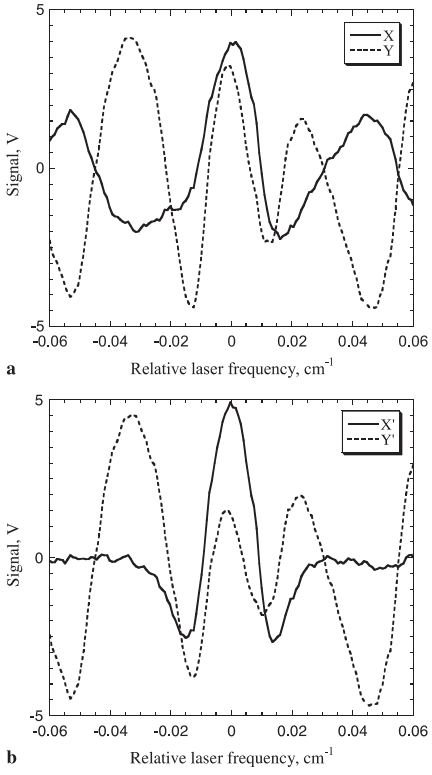

FIGURE 3 **a** Experimentally acquired QEPAS data of CO doped propylene; **b** same data set after reference frame rotation. *Horizontal scale* 0 corresponds to center of CO R(14) absorption line at 2196.664 cm^1. The *vertical scale* represents the lock-in amplifier output voltage

quasi-continuous online measurements. This would require periodic detuning of the laser wavelength from the CO absorption peak to one of the sufficiently distant C_3H_6 peaks and a subsequent adjustment of the lock-in amplifier phase to zero out the X' component.

In order to calibrate the sensor and determine the angle φ_2, pure CO was added to the original gas sample so that the resulting CO concentration became much higher than 5 ppmv. The measurements were performed as previously at 50 Torr pressure. Figure 4 shows the observed CO signal projection to X' ($\alpha = 23.3°$) at the R(14) line center as a function of CO concentration derived from dilution factor. The calibration coefficient calculated from the linear fit of these data yielded a CO concentration of 7.0 ± 0.5 ppmv in the original gas sample. The angle $\varphi_2 = 65.9 \pm 0.3°$ was found to be the same for all CO concentrations, and $\varphi_1 = 111 \pm 1°$ as measured in the same experimental run. Thus, $\theta_2 > \theta_1$ as shown in Fig. 1, and according to (1) the thermalization of vibrational CO excitation in propylene is slower than thermalization of the optically excited C_3H_6. Most probably the first step of CO relaxation is the energy transfer to a manifold of C_3H_6 rovibrational states.

A knowledge of the instrumental lag ψ is required to obtain complete phase information. In our system the identified sources of phase delays which are not $\pi/2$ multiples are:

1. electronic delay between the sine wave source (function generator) and laser current modulation;
2. phase lag between the laser current modulation and wavelength modulation;
3. phase shift between the thermal energy input and pressure in the acoustic microresonator

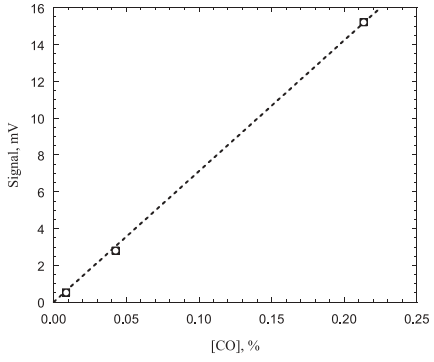

FIGURE 4 Peak intensity of the QEPAS signal projection to X' (same reference frame rotation as in Fig. 3b) as a function of CO concentration in propylene. *Vertical scale* is the transimpedance preamplifier output (preamplifier feedback resistor is 10 MΩ Linear fit is forced through zero

While the phase lags (1) and (2) are constant and can be readily accounted for, phase shift (3) is pressure-dependent if the resonant frequency of the microresonator is shifted from f_0. Such a shift is quite possible, because the microresonator geometry differs from the ideal half-wavelength-long tube, and geometric tolerances are limited by the used assembly technology. Pressure variations change the microresonator Q-factor, which in turn influences the phase shift. Our observations indirectly confirm the ψ dependence on gas pressure. For example, the relaxation time τ calculated for NH_3 in N_2 based on the measured $\varphi(P)$ (unpublished data from [13]) assuming $\psi(P) \equiv$ const, was found to be 1.5 ms Torr. Such a slow relaxation would result in a 9 times signal drop when the gas pressure is changed from 760 Torr to 30 Torr, according to the factor $\frac{1}{\sqrt{1+\tan^2\theta}}$ [3]. This is in contradiction with experimental observations (see Fig. 3 of [13]). In addition, according to [14], V–T relaxation time of the lowest NH_3 vibration ν_2 is only 85 μs Torr. Energy transfer time from the vibrational state at $\sim 6500\,\mathrm{cm}^{-1}$ excited in [13] to translational motion should be about the same because of fast collision-induced intramolecular relaxation [15]. Therefore, the observed $\varphi(P)$ can not be explained by phase lag related to NH_3 relaxation.

The CO relaxation rate in propylene can be evaluated if additional assumptions are made. In [13] V–T relaxation of propylene is reported to be faster than 6 ns at room temperature and (presumably) atmospheric pressure. If we assume it to be instantaneous (that is, $\tau \ll 1/\omega$) at 50 Torr, then $\theta_2 = \varphi_1 - \varphi_2 \approx 45°$, and since the vibrational heat capacity of CO at room temperature is negligible, we obtain from (1) τ_{V-T} (CO-C_3H_6) $= \frac{\tan(45°)\ 50\ \mathrm{Torr}}{2\pi\ 32\,760\ \mathrm{Hz}} \approx$ 240 μs Torr.

Similar phase measurements were performed with N_2O doping of propylene by targeting the P(30) transition of the ν_3 mode at $2195.633\,\mathrm{cm}^{-1}$ [12]. Relaxation of N_2O in propylene was found to be much faster than CO, and the phase difference is noticeable only at $P \sim 10$ Torr or less. The plot in Fig. 5 shows $\tan(\varphi_1 - \varphi_2)$ as a function of pressure, index 2 now refers to N_2O. If we assume as before that $\theta_2 = \varphi_1 - \varphi_2$ and $C_{\mathrm{tr}}/C_0 \approx 0.8$ based on the data from [8], the linear fit shown in Fig. 5 yields τ_{V-T} (N_2O-C_3H_6) ≈ 9 μs Torr. The assumption of instant relaxation of C_3H_6 is less justified at lower pressures, which makes the N_2O relaxation time estimate less reliable than the estimate for the CO relaxation rate.

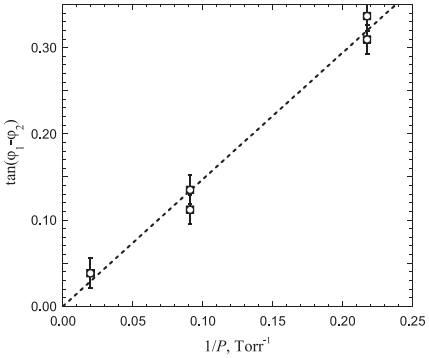

FIGURE 5 Tangent of the phase difference between N_2O and propylene photoacoustic signals as a function of the inverse pressure of the gas. Linear fit is forced through zero

A measurement of V–T relaxation rates was not the primary goal of this work. Unambiguous QEPAS-based phase measurements can be performed if the acoustic microresonator is removed from the sensor assembly, thereby eliminating the $\psi(P)$ dependence. However, this would result in ~ 10 times loss in detection sensitivity [11], which is not acceptable for trace gas sensing applications.

ACKNOWLEDGEMENTS The authors thank Prof. R.F. Curl for many useful discussions and Dr. Gerard Wysocky for providing multipass cell absorption data. The authors also gratefully acknowledge financial support from the National Aeronautics and Space Administration, the Texas Advanced Technology Program, the Robert Welch Foundation, the National Science Foundation, the Office of Naval Research via a subaward from Texas A&M University.

REFERENCES

1 T.W.J. Gadella: "Fluorescence Lifetime Imaging Microscopy (FLIM)", *Microscopy and analysis*, pp. 13–15, May 1997
2 G. Gorelik: Dokl. Akad. Nauk SSSR **54**, 783 (1946) (in Russian)
3 T.L. Cottrell, J.C. McCoubrey: "Molecular

energy transfer in gases", Butterworths, London 1961
4 P.V. Slobodskaya: Izvest. Akad. Nauk SSSR **12**, 656 (1948) (in Russian)
5 E. Avramides, T.F. Hunter: J. Chem. Soc., Faraday Trans. 2 **75** 515 (1979)
6 E. Avramides, T.F. Hunter: Chem. Phys. **74**, 25 (1983)
7 R.A. Rooth, A.J.L. Verhage, L.W. Wouters: Appl. Opt. **29**, 3643 (1990)
8 NIST Chemistry Webbook online, http://webbook.nist.gov/chemistry/
9 A.A. Kosterev, Y.A. Bakhirkin, R.F. Curl, F.K. Tittel: Opt. Lett. **27**, 1902 (2002)
10 A. Miklós, P. Hess, Z. Bozóki: Rev. Sci. Instrum. **72**, 1937 (2001)
11 D. Weidmann, A.A. Kosterev, F.K. Tittel: Opt. Lett. submitted
12 L.S. Rothman, A. Barbe, D. Chris Benner, L.R. Brown, C. Camy-Peyret, M.R. Carleer, K. Chance, C. Clerbaux, V. Dana, V.M. Devi, A. Fayt, J.-M. Flaud, R.R. Gamache, A. Goldman, D. Jacquemart, K.W. Jucks, W.J. Lafferty, J.-Y. Mandin, S.T. Massie, V. Nemtchinov, D.A. Newnham, A. Perrin, C.P. Rinsland, J. Schroeder, K.M. Smith, M.A.H. Smith, K. Tang, R.A. Toth, J. Vander Auwera, P. Varanasi, K. Yoshino: J. Quant. Spectrosc. Radiat. Transfer **82**, 5 (2003)
13 A.A. Kosterev, F.K. Tittel: Opt. Lett. submitted
14 F.E. Hovis, C.B. Moore: J. Chem. Phys. **69**, 4947 (1978)
15 A.A. Kosterev, A.A. Makarov, A.L. Malinovsky, E.A. Ryabov: Chem. Phys. **219**, 305 (1997)
16 W. Griffith: Appl. Phys. **21**, 1319 (1950)